Simple model of the interrelation between single- and multiwall carbon nanotube growth rates for the CVD process

R. F. Wood,[1,2] S. Pannala,[3,*] J. C. Wells,[2,3] A. A. Puretzky,[1,2] and D. B. Geohegan[1,2]
[1]*Materials Science and Technology Division, Oak Ridge National Laboratory, Tennessee 37831, USA*
[2]*Center for Nanophase Materials Sciences, Oak Ridge National Laboratory, Tennessee 37831, USA*
[3]*Computer Science and Mathematics Division, Oak Ridge National Laboratory, Tennessee 37831, USA*
(Received 1 November 2006; revised manuscript received 15 February 2007; published 28 June 2007)

Recent time-resolved measurements of carbon nanotube (CNT) growth on Fe and Fe/Mo catalysts have identified a maximum growth rate and temperature corresponding to the onset of small-diameter, single-wall CNT (SWNT) formation. A simple model described here emphasizes the essential role of the SWNTs in the growth process of CNTs. Remarkably, it shows that the growth rate (i.e., the time derivative of the length) of a multiwalled CNT is the same as that of a SWNT at the carbon flux and diffusion coefficient corresponding to a given temperature. Moreover, below ~700 °C, the temperature above which SWNT growth is observed for a 6 sccm (cubic centimeter per minute at STP) C_2H_2 flow rate, the number of walls as a function of temperature is uniquely determined by the interplay of the incident flux of atomic C and diffusion rates consistent with *bulk* diffusion. Even partial melting of the catalytic particle is unnecessary to explain the experimental results on growth rate and number of walls. Above 700 °C, where severe catalyst poisoning ordinarily begins, the growth rate without poisoning is consistent with recent results of Hata and co-workers [Science **306**, 1362 (2004); Phys. Rev. Lett. **95**, 056104 (2005)] for "supergrowth."

DOI: 10.1103/PhysRevB.75.235446 PACS number(s): 81.07.De, 61.46.Fg, 81.07.Bc, 81.15.Gh

I. INTRODUCTION

Until recently, the growth rates of carbon nanotubes had not been generally measured *in situ* and could only be deduced indirectly after the samples had cooled to near room temperature. Consequently, the growth rates reported in the literature have varied over a broad range, making it difficult to distinguish the effects of various parameters on the growth dynamics. Results of accurate *in situ* time-resolved measurements are invaluable for modeling of the growth process and hence for a fundamental understanding of how to control it. In this paper, it is demonstrated that modeling of recent results by Puretzky *et al.*[1] obtained from time-resolved reflectivity (TRR) methods leads to unexpected insights into the growth dynamics. The close interrelationship between single-wall carbon nanotube (SWNT) and multiwall carbon nanotube (MWNT) growth is also emphasized. Also, recently Hata and co-workers[2,3] have observed growth rates an order of magnitude higher than those of Ref. 1, a result consistent with the calculations presented here.

While the use of time-resolved spectroscopy to study growth phenomena in carbon nanotube (CNT) research is not entirely new,[4] it is only recently that reasonably reliable techniques have been developed. Bonard *et al.*[5] used *in situ* field-emission spectroscopy directly in a chemical-vapor deposition (CVD) reactor at very low pressures. Growth rates as high as 10 μm/s were extracted but the reliability of these results has been questioned. More recently, Geohegan *et al.*[6] and Kim *et al.*[7] have introduced optical techniques for *in situ*, time-resolved measurements. Helveg *et al.*[8] used atomic-scale transmission electron microscopy to observe *in situ* the growth of carbon nanofibers. It appears likely that the growth modes of nanofibers are significantly different from those of nanotubes with only a few walls. In Ref. 1, the growth of dense forests of vertically aligned CNTs formed by CVD was studied using TRR measurements and rate equation (RE) analysis. The results of these experiments and calculations, briefly summarized next, will be our main focus. In this paper, we focus on the kinetics and the bulk diffusion processes (unlike the invocation of fast diffusion in highly disordered molten state in Ref. 1) which define the number of nanotube walls and growth rates.

The lengths of the CNTs as a function of temperature T were determined from the heights of the dense forest of nanotubes above the substrate on which they were formed. The growth rates were obtained from the derivatives of these lengths without regard to the number of walls in the tubes. At temperatures below about 700 °C, the growth with time was found to have an initial transient followed by a period of either linear or relatively constant increase after which a slow decrease ensued. This decrease is a common phenomenon and is usually attributed to "poisoning" of the catalyst, perhaps by the growth of a "carbonaceous" or amorphous C (*a*-C) layer on the surface of the catalyst, or by carbide formation inside or on the surface of the catalyst.

For a flow rate of 6 sccm (cubic centimeter per minute at STP), growth rates were observed to peak sharply at ~700 °C. Above this temperature, a much stronger poisoning mechanism, whose origin is still uncertain, rapidly decreased the growth rate. Raman scattering and high-resolution transmission electron microscopy were used to determine the number of walls in the CNT. At $T \sim 575$ °C and a flow rate of 2 sccm, the nanotubes had between five and ten walls, whereas at ~700 °C they were either single or double walled. The growth of these high-quality vertically aligned carbon nanotube arrays suggests a high degree of uniformity in the catalyst material and experimental conditions.

In the extensive RE analysis of their results, Puretzky *et al.*[1] first considered the flux of the carbon feedstock gas onto the surface of the metal catalyst. The flux of C atoms was estimated as

$$F_{c1} = F_{b1} p_1 e^{(-E_{a1}/k_B T)}, \tag{1a}$$

with

$$F_{b1} = 0.25 S_0 n_0 (k_B T / 2\pi m)^{1/2}, \tag{1b}$$

where F_{b1} is the incident molecular flux; p_1 contains the sticking coefficient, geometric factors, etc.; E_{a1}, the activation energy for catalytic decomposition of the feedstock material, was found by fitting the experimental data to be approximately 0.60 eV; S_0 is the surface area of the nanoparticle; n_0 is the partial density of C_2H_2 in the molecular flux; and m is the C_2H_2 mass. The parameter n_0 is particularly important because it provides a means for varying the incident C flux other than by changing the temperature and it is easily adjusted in the experiments. After the C atoms are produced on the surface, there are two main pathways for the process to proceed in the low-T regime: one by surface-bulk penetration of carbon into the catalyst where it can diffuse and the other by the formation of a carbonaceous or a-C layer that results in the long-term poisoning. The two processes occur on widely different time scales, both of which are much shorter than the resolution of the experiments. In fact, the amount of the incoming flux that forms the poisoning layer is quite small compared to the amount going into the catalyst for CNT growth. Hence, in the low-T regime the process described by Eq. (1) is expected to be the rate-determining step for the C flux introduced into the catalyst. As discussed at length in Ref. 1, there is also a time dependence introduced by the finite time it takes the carrier gas to move through the furnace tube to the CVD sample.

The high-T poisoning was taken into account by introducing a rate equation for the growth of the number of C atoms involved in the poisoning. This number was found to be a strong function of T with an activation energy of ~2.4 eV. Consequently, its effect for $T < 700$ °C is practically negligible while being of crucial importance at higher temperatures.

In Ref. 1, diffusion of C through the nanoparticle after penetration of the surface was treated simply by introducing the rate constant $k_t = D/R^2$, with D the *bulk* diffusion coefficient and R the radius of the nanoparticle. Finally, the number of shells in the CNT was determined by the concentration of carbon atoms on the surface of the catalyst nanoparticle expressed as the number of carbon monolayers.

We begin in the next section the description of the work presented here with some considerations based on the idea that the growth of MWNTs is intimately related to the growth of the SWNT at the same temperature. An expression for the number of walls that are formed is derived without invoking any consideration of melting. In Sec. III, a RE analysis similar to that developed by Puretzky *et al.*[1] is introduced. In Sec. IV, various calculations using the two-dimensional (2D) diffusion equation are described. These calculations give support to the approximation that the gas-phase dynamics simply provides boundary conditions for solution of the diffusion equation in the catalytic particle. The paper concludes with a brief summary and discussions of what we suggest are some of the implications of our work.

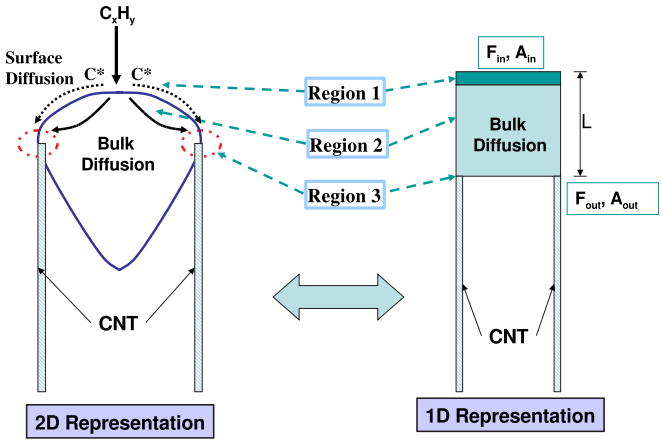

FIG. 1. (Color online) Tip-growth mechanism. This was originally proposed by Baker *et al.* for carbon nanofibers and later used for growth of CNTs. The immediate vicinity of the catalyst particle is divided into three distinct regions for convenience. Region 1 includes decomposition of carbon, carbonaceous layer or other poisoning mechanisms, possible carbide layer, etc. Region 2 represents the internal processes (such as diffusion) within the catalyst. Region 3 is located where the carbon gets incorporated into the CNT. The figure also shows how the 2D solution is mapped to the 1D solution methodology.

II. SWNT GROWTH AND THE NUMBER OF WALLS

The conceptual model (Fig. 1) assumed here is the same as that first discussed by Baker *et al.*[9] and subsequently used by many other groups[10–12] for both nanofiber and nanotube growth. Briefly stated, a carbon-containing compound is "cracked" on a nanoparticle catalyst and the atomic carbon diffuses into and through the solid to the sites where the nanotube grows. It is widely observed that on a well-prepared catalytic particle, the radius of the CNT is essentially the same as that of the particle. This is assumed here. It is reasonable because the strain energy of curvature decreases rapidly with increasing tube radius.[13] Also, for most nanoparticle shapes the diffusion path to the growth sites is minimized. We emphasize that in this paper, "SWNT" always refers to the CNT with a single wall and with radius equal to that of the nanoparticle.[14] An earlier paper[15] provides a more specific description for the numerical 2D diffusion calculations to be discussed in Sec. IV.

The steady-state[16] form of the 2D diffusion equation is

$$\partial/\partial r[rD(T)\partial Y_C/\partial r] + \partial/\partial z[rD(T)\partial Y_C/\partial z] = 0. \tag{2}$$

For isotropic diffusion, the concentration Y_C does not depend directly on the diffusion coefficient $D(T)$ but it does via the boundary conditions. At the position where the CNT is growing, the flux out of the catalytic particle is given by

$$F_{out} = D(T)[\, n_r \partial Y_C/\partial r|_{out} + n_z \partial Y_C/\partial z|_{out}], \tag{3}$$

where n_r and n_z are unit vectors along r (radial) and z (axial) directions. To simplify the discussion and for comparison with the rate equation approach, we consider only the one-dimensional (1D) case given by the axial term, i.e.,

$$F_{out} = D(T)\partial Y_C/\partial z|_{out}. \quad (4)$$

Values of $D(T)$ are readily found in the literature, but an approximate expression for the concentration gradient is also required. In the systems considered, the size and composition of the catalytic particle should remain virtually the same for all T during an experiment and need not be considered further here.

The flux boundary condition at the inlet boundary will determine the carbon influx and thus control the rate of CNT growth. This is a Neumann (gradient) boundary condition to Eq. (2) of the following form:

$$\partial Y_C/\partial z|_{in} = F_{in}/D(T), \quad (5)$$

where F_{in} is the input carbon flux at the interface of regions 1 and 2 of Fig. 1.

The results from the steady-state 2D diffusion calculations of Sec. IV provide a guide for the choice of approximate forms of $\partial Y_C/\partial z$. The simplest and most reasonable approximation to make is the linear variation of the concentration in the axial direction through the 1D catalyst rod of uniform diameter. This assumption would lead to the condition that the concentration gradient is constant along the catalyst particle. This, in turn, would mean that

$$\partial Y_C/\partial z|_{out} = \partial Y_C/\partial z|_{in}. \quad (6)$$

From Eqs. (4)–(6), we have

$$F_{in} = F_{out}. \quad (7)$$

This is an obvious result as the mass has to be conserved for this steady-state scenario. However, we have to account for the area change between the inlet and outlet. Considering the area difference for the CVD CNT process as depicted in Fig. 1, we have the following relation by adding the CVD subscript for clarification:

$$F_{out,CVD} = (A_{in}/A_{out})F_{in,CVD} = AF_{in,CVD}. \quad (8)$$

$F_{in,CVD}$ is a temperature-dependent function which depends on the concentration of the carbon-containing gas, the temperature of the furnace, and the presence of the poisoning layer. We write $F_{in,CVD}$ in terms of concentration of the C-containing molecules in the incoming gas stream, given by n_0, and the rest of the physical mechanisms controlling the input carbon flux are lumped into the temperature-dependent function, $f_{in,CVD}(T)$. This is only a manipulation to isolate the effects of n_0 as that can be controlled in the experiments as a separate parameter from the furnace temperature. With this notation, Eq. (8) can be written as

$$F_{out,CVD} = n_0 f_{in,CVD} A. \quad (9)$$

When all poisoning effects are neglected, $f_{in,CVD}(T)$ is extracted in a straightforward fashion from Eqs. (1a) and (1b). By variation of n_0, a family of CVD growth curves can be generated, as illustrated in Ref. 1 and demonstrated in the next section. When poisoning is included, an effective form of $f_{in,CVD}$ from a solution of the rate equations must be used.

We now specifically consider SWNT growth. The experimental determination of T_m, the temperature at which the maximum growth rate of a SWNT occurs under the given conditions, is essential to our approach. Applying Eq. (4) for SWNT growth and adding the subscript SW to stand for SWNT, we get

$$F_{out,SW} = D(T)(\partial Yc/\partial r)_{SW} = D(T)A_{SW}F_{in,SW}(T)/D(T) = A_{SW}B_{SW}f_{in,SW}(T). \quad (10)$$

$f_{in,SW}(T)$ is the input flux to grow a SWNT and its form has not yet been specified. B_{SW} is a "normalization" constant introduced to ensure that $F_{out,SW}$ and $F_{out,CVD}$ will be equal at T_m for a given value of n_0. It is important to understand the role of B_{SW} and the introduction of this approach should become more obvious in the next section. Hidden within this constant are the kinetics of the atomic interactions at the growth interface, which determine whether a SWNT will continue to grow or inner walls will begin to form to yield a MWNT. Since the complex atomistic calculations that would yield those kinetics are not yet possible, the experimental results must be used. From Eq. (10),

$$B_{SW} = F_{out,SW}(T_m)/[A_{SW}f_{in,SW}(T_m)] = F_{out,CVD}(T_m)/[A_{SW}f_{in,SW}(T_m)]. \quad (11)$$

The last equality follows from the requirement that $F_{out,SW}$ and $F_{out,CVD}$ be equal at T_m. Again, from mass conservation, $F_{out,CV}A_{out,SW}=F_{in,\mathrm{CVD}}A_{in}$ and then

$$B_{SW} = F_{in,CVD}(T_m)A_{SW}/f_{in,SW}(T_m)D(T_m) = n_0 F_{in,CVD}(T_m)/f_{in,SW}(T_m). \quad (12)$$

A_{in} is the area on which the incident flux falls and $A_{out,SW}$ is the annular area from which the SWNT grows. It should be noted that $F_{in,CVD}$ in this equation contains the specific value of n_0 used in the experiments to determine T_m, i.e., 6 sccm.

To obtain the optimum growth rate of a SWNT, we need to adjust $\partial Y_C/\partial z$ via $f_{in,SW}(T)$ in Eq. (10). We have studied two functional forms (exponential dependence on temperature typical of any activation barrier) for $f_{in,SW}(T)$, namely,

$$f_{in,SW}(T) \sim D(T) \quad (13)$$

and

$$f_{in,SW}(T) \sim f_{in,CVD}(T)D(T). \quad (14)$$

These were chosen because the total activation energies are known and they are both greater than $f_{in,CVD}$ alone. The proportionality constants must be chosen to give the dimensions of flux. The second form yields a higher growth rate than the first, but without further experimental input, a choice between the two cannot be made. In fact, calculations carried out with both yield very similar results that fall within the accuracy of the experimental data. The form in Eq. (14) will be used for the calculations reported here.

Next, we make the plausible assumption that the flux to grow a CNT with N_w walls can be expressed in terms of $F_{out,SW}$, the flux required to grow a SWNT at that temperature. (The validity of this assumption will be substantiated later by the agreement with experiment.) The simplest choice would be to put $F_{out}=N_wF_{out,sw}$, but it would be too simple. It does not take into account that the radius of each successive wall is decreased by ΔR, the interlayer spacing. Instead, we

need to consider the contribution of the individual walls and then sum over them. In the experiments, the incoming flux is considered to be uniform over the top surface of the catalytic particle. Let $N_{C,out}$ be the total number of C atoms/s flowing out of the catalyst into the growing CNT and let $N_{C,SW}$ be the corresponding value for a SWNT. We put

$$N_{C,out} = F_{out,SW}(A_1 + A_2 + \cdots + A_{NW}) = N_{C,SW}(1 + A_2A_1 + \cdots + A_{NW}/A_1). \quad (15)$$

A_i is the annular area of the ith wall of radius R_i and thickness ΔR. A_i is equal to $2\pi\Delta RR_i$. ΔR is taken to be the interplanar spacing in the c direction of graphite. The SWNT has the maximum radius with $R_1=R$ and $A_1=2\pi\Delta RR_1$ so that $N_{C,SW}=F_{in}A_1$. Then,

$$N_{C,out} = N_{C,SW}\{1 + (R-\Delta R)/R + (R-2\Delta R)/R + \cdots + [R-(N_W-1)\Delta R]/R\} = N_{C,SW}\{N_W - [1+2+\cdots+(N_W-1)]\Delta R/R\}. \quad (16)$$

The sum in square brackets is simple and results in the expression

$$N_{C,out} = N_{C,SW}[N_W - (N_W-1)N_W\Delta R/2R]. \quad (17)$$

Again, putting $N_{out}=N_{in}$ and with $R_p \equiv 2R/\Delta R$, this equation can be solved for N_w to get

$$N_W = 0.5(1+R_1) \pm 0.5[(1+R_p)^2 - 4R_pN_{C,in}/N_{C,SW}]^{1/2}. \quad (18)$$

When $N_{C,in}=N_{C,SW}$, $N_w=1$ as it should. However, as $N_{C,in}/N_{C,SW}$ becomes larger than 1 with decreasing T, the number of walls grows faster than $N_{C,in}/N_{C,SW}$ because of the decreasing radii of the inner shells, but there is a limit on the number of walls that can be grown before the argument of the square bracket becomes negative. This limit is just the number that can fit into R, i.e., $R/\Delta R$. In the present case, with $R=5$ nm and $\Delta R=0.335$ nm, $N_{W,max}\approx 15$. However, it is unlikely that the innermost walls can form because nanotubes smaller than $R\sim 1$ nm have not been observed. A more likely limit is 10–12 for the walls, but then the cores may have C in some other form such as a-C.

III. CALCULATIONS OF GROWTH RATES AND NUMBER OF WALLS

Application of the above equations is straightforward and can be illustrated using the rate equation approach from Ref. 1 summarized in the Introduction. We define $F_{in,CVD}$ by Eq. (1), namely,

$$F_{in,CVD} = F_{c1} = 0.25S_0n_0(k_B/2\pi m)^{1/2}p_1T^{1/2}\exp(-E_{a1})(k_BT) = n_0f_{in,CVD}(T), \quad (19)$$

The incoming flux is for C atoms that are actually incorporated into the nanoparticle. A small fraction of the C that produces long-term poisoning will be neglected. Also, S_0 is the area of the nanoparticle so that in these equations the flux is for the actual assumed area rather than for the unit area.

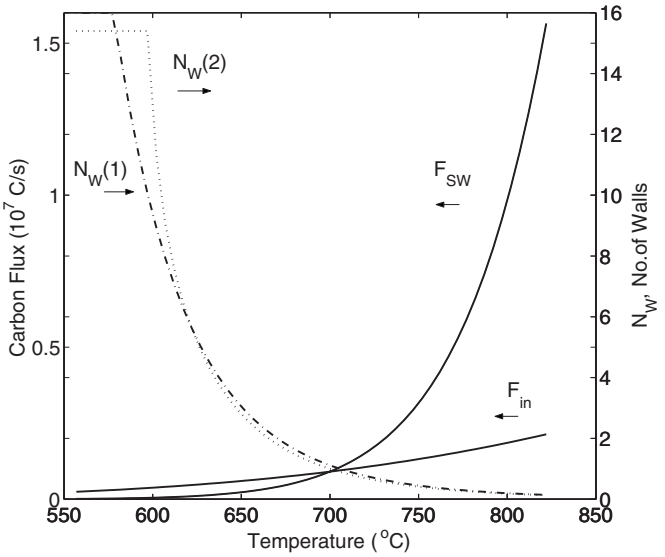

FIG. 2. Comparison of the incoming CVD flux, denoted here by F_{in}, and that required to grow a SWNT (here denoted by F_{SW} and in the text by $F_{out,SW}$) as a function of temperature. Also shown is the number of walls as calculated from Eq. (10). At 700 °C, the two fluxes are just equal and so a SWNT grows. For $T<700$ °C, the CVD flux exceeds the diffusion flux and multiwall tubes form. For $T>700$ °C, only SWNTs grow but the growth rate is greatly reduced because the CVD process does not supply enough carbon.

Consider first the growth of a SWNT in the temperature range below 700 °C. The radius of the nanotube, the areal density of C atoms (3.82×10^{15}/cm^2) in graphene, the diffusion coefficient, and the inlet flux are known. Also, from the experiments the maximum growth rate and the temperature T_m, at which it occurs, have been established for the SWNT growth. As already mentioned, the T dependence of the inlet flux is $\sim\exp(-0.60\ \text{eV}/kT)$.[1] For the diffusion rate of C in bulk Fe,[17,18] $D_0=0.1-0.5$ cm^2/s and the activation energy is 1.4–1.6 eV.

Figure 2 gives the results for $F_{in,CVD}$, $F_{out,SW}$, and N_W from Eqs. (19), (10), and (18), respectively. By comparing $F_{out,SW}$ to $F_{in,CVD}$, it is seen that for $T<700$ °C, the CVD flux is too large for only a SWNT to grow at steady state even at the maximum rate that has been established. Consequently, first tubes with two, then three, etc. walls must begin to form. The number of walls at any T is given by Eq. (18), which involves only the ratio $N_{C,in}/N_{C,SW}$ and the radius. On the other hand, in the high-T regime above 700 °C, $F_{in,CVD}$ has fallen below $F_{out,SW}$. This means that not enough carbon is being supplied to grow a SWNT at the optimum rate for these temperatures even when high-T poisoning is not considered. In this model, only SWNTs are formed in this high-T regime and generally grow at less than the maximum rate. The rate that could be achieved if C was supplied at the optimum rate is quite high; we will return to this in the last section.

The curve labeled $N_W(1)$ in Fig. 2 shows the number of walls as a function of temperature obtained by following the fitting procedure of Ref. 1, to which we refer the reader for the details. There is no natural cutoff in N_W at low temperatures. Curve $N_W(2)$ gives the number of walls obtained from Eq. (18). There is a natural cutoff in $N_W(2)$ as T is lowered

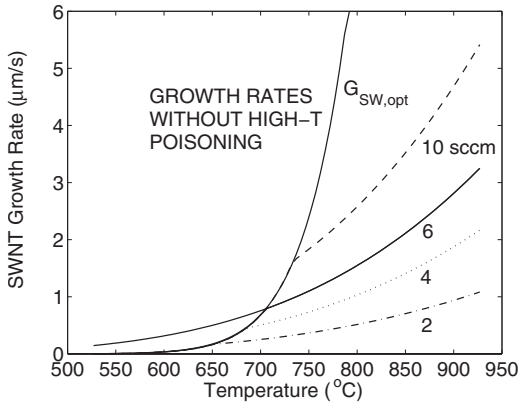

FIG. 3. Computed growth rates as a function of temperature and the inlet carbon concentration. High-temperature poisoning is not considered. $G_{SW,opt}$ is the curve for optimal SWNT growth extended to higher temperatures. To the right of this curve the growth is controlled by the rate of supply of C by the CVD process, while to the left it is controlled by the growth rate of a SWNT. The curve for the CVD supply of C for the 6 sccm has been extended to lower temperatures to emphasize that in this region multiwalled tubes are being grown albeit at the SWNT growth rate.

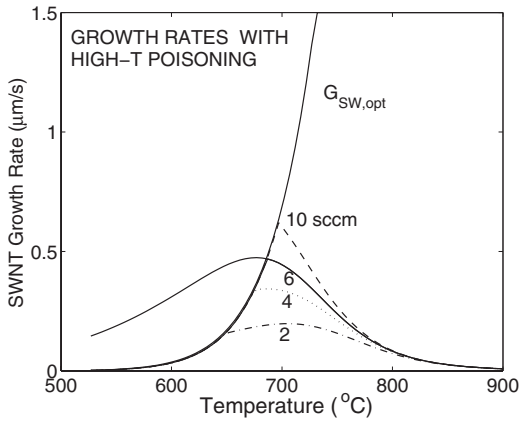

FIG. 4. The same curves as those in Fig. 3 but with high-temperature poisoning included. Again, it can be seen that the growth rate in the low-T region is controlled by the SWNT growth rate even though multiwalled tubes are grown. Of course, in the high-T region only SWNTs grow but not at the maximum rate because the CVD process does not supply C fast enough. $G_{SW,opt}$ has the same meaning as in Fig. 3.

and there is no need to introduce the fitting procedure described at length in Ref. 1 or the need to introduce near melting in a highly disordered region.

We emphasize that N_W is not required to be an integer, which suggests some interesting consequences. Except for the SWNTs, the innermost wall of all MWNTs may be defective, and often quite so. For example, for $N_W=2.5$ two essentially perfect outer walls might be expected, but with the third wall half filled with C vacancies and catalytic atoms incorporated into that wall. This is obviously too complex an issue to be interpreted based solely on continuum calculations and other explanations involving atomistic processes can surely be developed.

Figure 3 depicts how the SWNT growth rate varies with temperature as the incoming flux of C is changed via the parameter n_0. In these calculations, the high-T poisoning is still not included. The curve labeled $G_{SW,opt}$ (which can be obtained from $F_{out,SW}$ through a conversion factor) shows the growth rate when the supply of C is exactly optimum to form a SWNT. To the right of this line, SWNTs still form but the growth rate is slowed because C is not supplied fast enough to keep pace with the temperature dependence of diffusion. In the case of 6 sccm flow rate, the growth curve has been extended to lower temperatures to the left of the $G_{SW,out}$ line. At these temperatures, multiwalled nanotubes are formed and the number of walls can be determined via Eq. (18). However, even in these lower-T regions the lengths of the MWNTs are determined by the growth rate of the SWNT, as will be demonstrated shortly.

The growth rates in the more complex case when high-T poisoning is allowed can be found by including the relevant terms in the system of rate equations and repeating the calculations leading to Fig. 3 for all temperatures. The results are shown in Fig. 4. The curves were obtained by first solving the full set of rate equations including the term which gives the time dependence of the source expansion mentioned in the Introduction. The maximum CNT growth rate with respect to time for the range of temperatures indicated was then determined. The very quick onset of poisoning above 700 °C is striking. The extension to the left of the curve labeled 6 sccm beyond the $G_{SW,opt}$ curve was generated from the rate equations by determining the atomic C concentration at the catalyst-gas phase interface. It reflects the effects of poisoning which drastically reduce the amount of atomic carbon that enters the catalyst particle. The curve labeled $G_{SW,opt}$ was generated from the gradient of the C concentration and the diffusion coefficient as in Eq. (4). It is plotted here to show how closely it coincides with the growth rate curve, including poisoning, in the region below 700 °C. There is no difference between the two curves to within the accuracy of the experimental data. This indicates that in this low-temperature regime, *multiwalled CNTs are growing at the (temperature dependent) maximum rate of SWNTs*.

Figure 5 shows the data from Fig. 4 for the 6 sccm case compared to the experimental data taken directly from Fig. 13 of Ref. 1. A small adjustment has been made to both calculated curves to bring them into closer coincidence with the experimental data. This was done simply by varying the number of C atoms per micron of SWNT growth and has no fundamental significance since the areal density of C in graphite sheets is well established. The purpose of this figure is to demonstrate that *the growth rates of all the CNTs grown really are controlled by the SWNT rate*. The solid curve was generated by the calculations of Ref. 1 which assume melting or near melting to obtain the number of walls, while the dashed curve was obtained from the calculations described here that assume only solid-state diffusion throughout. Again, the differences between the two curves are hardly discernable.

Before turning to calculations with the 2D diffusion equation, it is interesting to consider the results of Hata and co-workers[2,3] and ask if a growth rate of $\sim 2\ \mu$m/s for

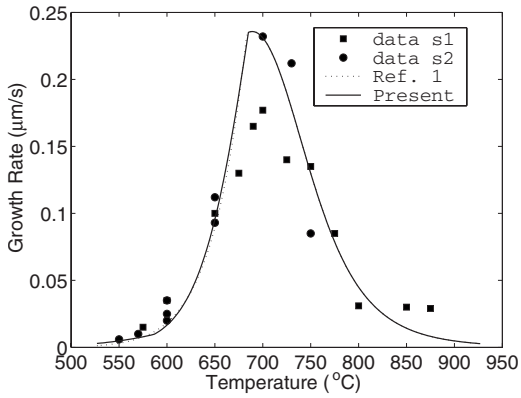

FIG. 5. Comparison of the calculated growth rates with the experimental data. The calculated curves have been adjusted to provide close agreement with the experimental data, as discussed in the text.

SWNTs is possible from these calculations once the high-T poisoning is eliminated. In Fig. 3, it can be seen that if C is supplied at a fast enough rate at $T \sim 750$ °C there is no difficulty in attaining very high growth rates. However, solubility limits, melting of the CNT, etc., can be expected to come into play. It would require a flux of C atoms into the CNT of 2.4×10^6 C/s to achieve ~ 2 μm/s. We estimated the upper limit imposed by solubility considerations to be $\sim 10^6$ C/s for Ni (Ref. 19) and it could easily be higher for Fe and Fe compounds.

IV. DIFFUSION CALCULATIONS

The numerical techniques used in the 2D diffusion work are the same as those of Ref. 15, although the shape of the nanoparticle has been changed to that shown in Fig. 6. This shape is probably more representative of the particles prepared by premelting thin metallic films deposited on insulating substrates, as is commonly done in most CVD experiments. Also, it readily shows the likely symmetry between tip- and root-growth modes. In the actual calculations, the axial symmetry of the problem is fully utilized. The small stub of a SWNT shown on the figure is introduced primarily to facilitate the calculation of the C flux into the growing nanotube and the gradient of the concentration.

As in Ref. 15, the sample is divided into three main regions (see Fig. 1 for a schematic). The gas-phase reactions above and at the catalytic particle's surface and the formation of solid-phase compounds at that surface are confined to region 1. Whereas little information about these processes was available previously, the work of Ref. 1 has enabled many of them to be included in a quantitative analysis. We find that the most important of these processes can be incorporated as boundary conditions on region 2, where the diffusion equation in the nanoparticle is actually solved. Region 3 is the interface between the catalyst and the nanotube and though little is still known about it in detail, it appears from first-principles calculations[20–23] that the bonding between carbon and transition metals that form good catalysts is nearly as strong as the C-C bonding in the nanotubes. The C atoms are able to make a transition from the nanoparticle to the nanotube without having to overcome a significant activation barrier.

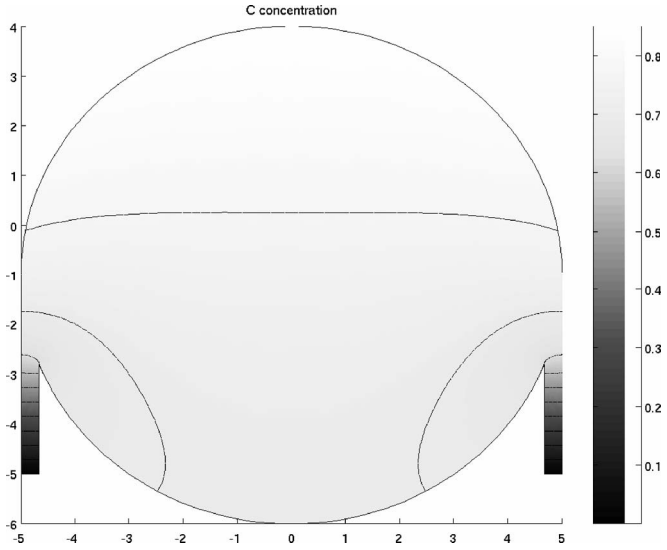

FIG. 6. Spherical nanoparticle shape used in the diffusion calculations. The axial symmetry evident in the figure is utilized throughout the actual calculations. The nanotube "stubs" are used to aid in the calculation of the fluxes. The color bar indicates that the concentration is quite uniform throughout most of the catalytic nanoparticle and the variable u represents the carbon concentration.

In Ref. 15, the boundary condition (BC) at the top surface was taken in the Dirichlet form in which the mass fraction of *atomic* carbon was fixed even though the temperature was varied. However, in a CVD process the mass fraction at the top surface cannot be held fixed easily while the temperature of the catalyst is varied. Instead, a flux BC can be introduced and the T variation taken from the results of Ref. 1, or more explicitly, from Eq. (19). A flux BC at the outlet position where the SWNT is growing could also be introduced but it was found to lead to numerical instabilities. Therefore, the assumption in Ref. 15 of a mass fraction of 0.001 where a nanotube is growing (the exact value used is not critical) was used. At all other positions, the flux into or out of the particle is zero.

In Fig. 6, the concentration of C in the catalyst during the growth of a SWNT at 700 °C on a particle of 5 nm radius is shown. The flux was chosen to give the optimal growth rate (see Fig. 3) for a flow rate of 6 sccm. The horizontal scale is in nanometers and in the calculations the thickness of a wall is taken to be 0.335 nm, the interplanar separation along the c axis in graphite. In the vertical spectrum bar at the right, it can be seen that the C concentration at the top of the catalyst is ~ 0.80 C/nm^3 or $\sim 8 \times 10^{20}$ C/cm^3. There are 8.50×10^{22} Fe atoms in a cm^3 so the atomic fraction is $\sim 0.95 \times 10^{-2}$ and the mass fraction is 0.002.

Now, exactly the same diffusion calculation (T, flux, etc., unchanged) can be carried out for a MWNT, e.g., with four walls. From such a calculation, the length of this MWNT increases at approximately a quarter of the rate of the SWNT. At first sight, this seems reasonable but it is in disagreement with the experimental results in Fig. 5. According to our model, it is not possible to grow a MWNT under exactly the

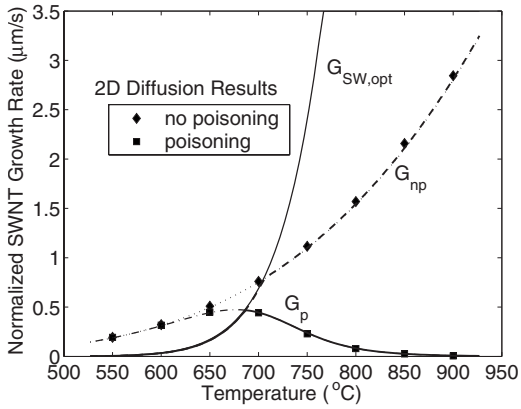

FIG. 7. Results of rate and diffusion equation calculations. G_{np} and G_p are the growth rates without and with poisoning, respectively. The squares and diamonds give the corresponding results from the 2D calculations. To the left of the $G_{SW,opt}$ curve, the growth rates are normalized to that for SWNT growth. See text for further details.

same conditions used for the growth of a SWNT. The only way to grow a multiwalled tube on this nanoparticle is to increase the incident flux (via the flow rate) at 700 °C or reduce the growth temperature, as dictated by data like those in Fig. 2.

Some results from the 2D diffusion calculations are summarized in Fig. 7. We define a "normalized" SWNT growth rate by dividing the number of C atoms per second going into the nanotube by 1.2×10^6, the number of atoms required to grow a SWNT of 5 nm radius at 1 μm/s. It is useful to do this because the diffusion calculation cannot determine the number of walls. On the figure $G_{SW,opt}$, the optimal growth rate of a SWNT, is repeated. To the left of this curve, the normalized growth rate gives the rate if all of the C atoms could be incorporated in a SWNT. However, a growth rate greater than $G_{SW,opt}$ at a given temperature cannot be achieved, so that CNT growing under these conditions must form MWNTs, as already discussed. The number of such walls is determined by dividing the normalized growth rate by $G_{SW,opt}$. The actual growth rate as a function of T is indicated by the heavier curves.

The calculated points shown by diamonds are for the case when high-T poisoning is not included. The T dependence of the input flux (top surface BC) is given by Eq. (19). For the more complicated case that high-T poisoning is included (triangles), the input C flux must be obtained from a solution of the full set of rate equations, which determines the T dependence of the poisoning function and therefore of the C flux on the top surface.

The agreement between the diffusion results and those from the rate equation approach is excellent. This reenforces our contention that solid-state diffusion is sufficient to explain the experimental results. It also seems to justify the assumption that the results of processes in region 1 can be incorporated simply by modifying the boundary conditions at the interface with region 2.

It should be understood, however, that the details of our model are tailored to the results of Ref. 1 and the extent to which the model may apply to other situations can only be determined after much more experimental and computational work.

V. SUMMARY AND DISCUSSION

An expression is derived for the growth of a MWNT in terms of the SWNT at the same temperature. The observed maximum growth rate of a SWNT at ~700 °C is used to calculate the T-dependent gradient of the concentration. This gives the SWNT growth rate at all other T and allows the number of shells to be calculated directly from the assumption of steady-state growth and without requiring melting to occur. The growth rate (rate of increase of length) of a multiwalled tube is the same as that of a SWNT at a given temperature. However, the innermost wall may be very imperfect. Inclusion of high-temperature poisoning produces growth rates almost identical to those of Ref. 1.

Calculations with the 2D diffusion equation demonstrate that high-T poisoning can be included via the BC at the top surface. The implication is that the poisoning mechanism operates just above and at the surface of the catalyst and not throughout any extended region in the catalyst itself.

A. Growth rate and $G_{SW,opt}$

The growth rates calculated here are a bit higher than the measured ones, but not as high as those of Ref. 1. In that reference, it was assumed that there are 10^{15} C atoms/cm^2 in a graphene sheet, but a more precise calculation gives greater than three times that number and this makes a significant difference in the calculated lengths. Even better agreement could be obtained by a slight modification of the input flux, but this would also require revising the treatment of the high-T poisoning term and this has not been done because of uncertainties in other aspects of the experiments and calculations. For example, what role does the nonuniformity of the growth rates across extended areas of the nanotube "blanket" play? Is "wiggling" of individual nanotubes important?

Our mapping out of the $G_{SW,opt}$ curve is dependent on only one experimental value at 700 °C and two assumptions and it would be very interesting to know how well our proposed curve agrees with experimental results at other temperatures.

B. Supergrowth

The growth rates for SWNTs obtained by Hata and coworkers when high-T poisoning is suppressed are not inconsistent with our calculations. Their experiments were carried out on Fe catalysts and the flow rates of ethylene (C_2H_4) they used were much higher than those for acetylene (C_2H_2) that were used in Ref. 1. Acetylene is known to be a much more efficient source of C than is ethylene for this type of experiment.[24] The radii and uniformity of size of the catalytic particles were not discussed in Ref. 2. We speculate that the upper limits on growth rates are probably determined by solubility limits and the tendency for nanotubes to begin to come apart at temperatures around 800 °C. However, there are substantial differences in the solubility of C in Ni and Fe compounds and it would be interesting to investigate the role

of the catalyst in "supergrowth." Also, Fig. 3 indicates that the flow rate must be carefully adjusted to the temperature in order to attain the maximum growth rate. On the other hand, if the flow rate is too great at a given temperature, multiwall tubes will begin to form.

C. Melting controversy

There is an ongoing controversy over the role of melting, or lack thereof, in CNT growth. Recently, many authors[25–28] have concluded that it is necessary to assume that the nanoparticle is molten or has a melted layer at the surface. Other works conclude that molten nanoparticles are not necessary and that surface diffusion processes dominate the growth kinetics.[29–32] The diffusion coefficients used in the present work are those appropriate to a solid, and apparently in the size range of the catalytic particles used there is no need to assume the much faster diffusion characteristic of a liquid or a highly disordered region. The conclusion that melting occurs is probably motivated in large part by the distortion of the catalytic particle that is observed in many experiments. We suggest that this elongation is caused by the strong bonding between the transition-metal atoms and the carbon atoms, together with the fact that at most temperatures the inner wall of the CNT is defective because of the growth dynamics spelled out by our model. We note that the authors of Ref. 2 did not observe any catalyst trapped in their rapidly grown SWNTs.

We also speculate that the growth mode observed for nanofibers[8] may be related to the tendency to incorporate catalyst atoms into the inner wall as suggested above. Clearly, the enormous fluctuation in the apparent size of the catalyst particle is not consistent with mass conservation unless the catalyst atoms are confined to a thin interfacial region. This makes our interpretation of our results in terms of a defective innermost wall, highly susceptible to the incorporation of metal catalyst atoms, more plausible.

ACKNOWLEDGMENTS

This research was supported by the U.S. Department of Energy under Contact No. DE-AC05-00OR22725 with the Oak Ridge National Laboratory, managed by UT-Battelle, LLC. This research was also sponsored by the DOE Office of Advanced Scientific Computing Research (S.P.) and funded by DOE Office of Basic Energy Sciences, Division of Materials Sciences and Engineering (D.B.G. and A.A.P.).

*Corresponding author. Email address: pannalas@ornl.gov

[1] A. Puretzky, D. B. Geohegan, S. Jesse, I. N. Ivanov, and G. Eres, Appl. Phys. A: Mater. Sci. Process. **81**, 223 (2005).
[2] K. Hata, D. N. Futaba, K. Mizuno, T. Namai, M. Yumura, and S. Iijima, Science **306**, 1362 (2004).
[3] D. N. Futaba, K. Hata, T. Yamada, K. Mizuno, M. Yumura, and S. Iijima, Phys. Rev. Lett. **95**, 056104 (2005).
[4] R. T. K. Baker, Carbon **27**, 315 (1989).
[5] J.-M. Bonard, M. Croci, F. Conus, T. Stockli, and A. Chatelain, Appl. Phys. Lett. **81**, 2836 (2002).
[6] D. B. Geohegan, A. A. Puretzky, I. N. Ivanov, S. Jesse, G. Eres, and J. Y. Howe, Appl. Phys. Lett. **83**, 1851 (2003).
[7] D. H. Kim, H. S. Jang, C. D. Kim, D. S. Cho, H. S. Yang, H. D. Kang, B. K. Min, and H. R. Lee, Nano Lett. **3**, 863 (2003).
[8] S. Helveg, C. Lopez-Cartes, J. Sehested, P. L. Hansen, B. S. Clausen, J. R. Rostrup-Nielsen, F. Abild-Pedersen, and J. K. Norskov, Nature (London) **427**, 426 (2004).
[9] R. T. K. Baker, M. A. Barber, J. J. Waite, P. S. Harris, and F. S. Feates, J. Catal. **26**, 51 (1972).
[10] I. Alstrup, J. Catal. **109**, 241 (1988).
[11] S. A. Safvi, E. C. Bianchini, and C. R. F. Lund, Carbon **29**, 1245 (1991).
[12] P. Chitrapu, C. R. F. Lund, and J. A. Tsamopoulos, Carbon **30**, 285 (1992).
[13] D. Tomanek, W. Zhong, and E. Krastev, Phys. Rev. B **48**, 15461 (1993).
[14] We believe that modifications of our approach could be used to treat other situations (e.g., nanofiber growth) but we have not yet studied these.
[15] S. Pannala and R. F. Wood, J. Nanosci. Nanotechnol. **4**, 4631 (2004).
[16] We use a steady-state approximation here because the experimental and computed growth rates have little meaning otherwise.
[17] O. A. Louchev, T. Laude, Y. Sato, and H. Kanda, J. Chem. Phys. **118**, 7622 (2003).
[18] W. L. Hsu, J. Appl. Phys. **72**, 3102 (1992).
[19] L. C. Isett and J. M. Blakely, Surf. Sci. **47**, 645 (1975); **58**, 397 (1976).
[20] Y. H. Lee, S. G. Kim, and D. Tomanek, Phys. Rev. Lett. **78**, 2393 (1997).
[21] F. Banhart, J.-C. Charlier, and P. M. Ajayan, Phys. Rev. Lett. **84**, 686 (2000).
[22] J. C. Wells, D. W. Noid, B. G. Sumpter, R. F. Wood, and Q. Zhang, J. Nanosci. Nanotechnol. **4**, 414 (2004).
[23] G. Kalibaeva, R. Vuilleumier, S. Meloni, A. Alavi, G. Ciccotti, and R. Rosei, J. Phys. Chem. B **110**, 3638 (2006).
[24] G. Eres, A. A. Kinkhabwala, H. T. Cui, D. B. Geohegan, A. A. Puretzky, and D. H. Lowndes, J. Phys. Chem. B **109**, 16684 (2005).
[25] V. L. Kuznetsov, A. N. Usoltseva, A. L. Chuvilin, E. D. Obraztsova, and J. M. Bonard, Phys. Rev. B **64**, 235401 (2001).
[26] O. Jost, A. A. Gorbunov, J. Moller, W. Pompe, X. Liu, P. Georqi, L. Dunsch, M. S. Golden, and J. Fink, J. Phys. Chem. B **106**, 2875 (2002).
[27] A. R. Harutyunyan, T. Tokune, and E. Mora, Appl. Phys. Lett. **87**, 051919 (2005); **86**, 153113 (2005).
[28] M. Lin, J. P. Y. Tan, C. Boothroyd, K. P. Loh, E. S. Tok, and Y-L. Foo, Nano Lett. **6**, 449 (2006).
[29] S. Hofmann, G. Csanyi, A. C. Ferrari, M. C. Payne, and J. Robertson, Phys. Rev. Lett. **95**, 036101 (2005).
[30] M. Cantoro, S. Hofmann, S. Pisana, V. Scardaci, A. Parves, C. Ducati, A. C. Ferrari, A. M. Blackburn, K.-Y. Wang, and J. Robertson, Nano Lett. **6**, 1107 (2006).
[31] F. Ding, A. Rosen, and K. Bolton, Carbon **43**, 2215 (2005).
[32] F. Ding, K. Bolton, and A. Rosen, Appl. Surf. Sci. **252**, 5254 (2006).